Electron and Proton Heating in Transrelativistic Magnetic Reconnection

arXiv:1708.04627

Michael E. Rowan[1], Lorenzo Sironi[2], and Ramesh Narayan[1] ([1]*Harvard*, [2]*Columbia*)

1 Introduction

The ultra-low-luminosity source at the center of the Milky Way, Sagittarius A* (Sgr A*), is thought to be powered by accretion onto a supermassive black hole. Sgr A* radiates well below the Eddington limit and there is strong evidence that the accreting gas can be described as an advection-dominated accretion flow (ADAF, also referred to as a radiatively inefficient accretion flow [RIAF]; Narayan & Yi 1994, 1995a, 1995b; Abramowicz et al. 1995; Narayan & McClintock 2008; Yuan & Narayan 2014). In ADAFs, the disk is geometrically thick and optically thin. Additionally, the plasma is predicted to be two-temperature for several reasons: first, in the ADAF configuration, the density of accreting gas is low enough that Coulomb collisions between electrons and protons are extremely rare on accretion timescales, so that the species become thermally decoupled. Second, electrons radiate more efficiently than protons. Lastly, relativistic electrons are heated less than nonrelativistic protons when subjected to the same adiabatic compression. For all these reasons, the plasma is expected to be two-temperature, with protons significantly hotter than electrons (Narayan & Yi 1995b; Yuan et al. 2003).

Despite the above arguments, the two-temperature gas may be driven to a single-temperature state by kinetic processes, such as reconnection and instabilities (Quataert et. al. 2002; Riquelme et al. 2012, 2015; Sironi 2015; Sironi & Narayan 2015; Werner et al. 2016). To capture the effects of these plasma processes, one requires a fully kinetic description, which can be achieved via numerical techniques such as particle-in-cell (PIC) simulations. In principle, such ab initio simulations can be used to provide the necessary subgrid physics that to date cannot be captured in magnetohydrodynamic simulations (e.g., Ressler et al. 2015, 2017; Ball et al. 2016, 2017; Chael et al. 2017; Sädowski et al. 2017).

In supermassive black hole accretion flows, the ratio of ion thermal pressure to magnetic pressure, $\beta_i=8\pi n_0 k_B T_i/B_0^2$, is expected to vary in the disk midplane in the range β_i~10-30. However, in plasma far above and below the midplane, i.e., the "corona," the system is expected to be magnetically dominated, such that $\beta_i<1$. Here, the dissipation of magnetic energy via reconnection can result in particle heating, acceleration, and bulk motion.

Even in the magnetized corona, the magnetization, $\sigma_i=B_0^2/4\pi n_0 m_i c^2$, is generally small, i.e., $\sigma_i\lesssim 1$. Electron heating by reconnection in the nonrelativistic limit ($\sigma_i\ll 1$) has been studied extensively, both theoretically and by means of PIC simulations, in the context of the solar wind, Earth's magnetotail, and laboratory plasmas (Hoshino et al. 2001; Jaroschek et al. 2004; Schoeffler et al. 2011, 2013; Loureiro et al. 2013; Dahlin et al 2014; Daughton et al. 2014; Shay et al. 2014; Haggerty et al. 2015; Li et al. 2015; Numata & Loureiro 2015; Le et al. 2016; Li et al. 2017). Though less commonly studied, relativistic reconnection (i.e., $\sigma_i\gg 1$) in electron-proton plasmas has also received some attention in recent years (Sironi et al. 2015; Guo et al. 2016). In this work, we study particle heating in the less explored transrelativistic regime (i.e., $\sigma_i\lesssim 1$).

2 Simulation Setup

We use the electromagnetic PIC code TRISTAN-MP to perform fully kinetic simulations of reconnection (Buneman 1993; Spitkovsky 2005). We employ 2D simulations, but all three components of velocity and electromagnetic fields are tracked. The initial field configuration is illustrated in the figure below. From the red to the blue region, the polarity of the inflow magnetic field reverses, as shown by the white arrows. The reconnection layer is initialized in Harris equilibrium. The field strength is parametrized via the magnetization $\sigma_w=B_0^2/4\pi w$, where B_0 is the magnitude of the magnetic field in the inflow region, and w is the enthalpy density per unit volume. We focus on antiparallel reconnection, and typically employ periodic boundary conditions along the x direction.

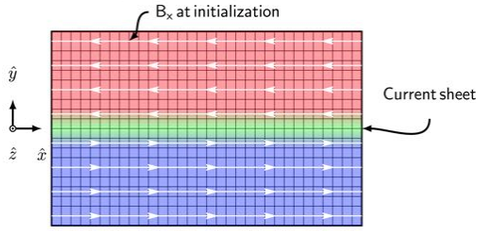

We investigate mass ratios m_i/m_e=10, 25, 50, and 1836 for β_i in the range 5e-4 to 2 (with fixed σ_w=0.1 and equal temperature ratio). With realistic mass ratios, we explore the β_i dependence of particle heating at higher values of the magnetization, σ_w=0.3, 1, 3, and 10. For our fiducial σ_w=0.1 and mass ratio up to the realistic value, we investigate temperature ratios T_e/T_i=0.1, 0.3, and 1.

3 Technique for Extracting Heating Efficiency

We characterize reconnection heating efficiency by the ratios $M_{Te,tot}=(k_B T_{e,down} - k_B T_{e,up})/(\sigma_i m_i/m_e m_e c^2)$ for electrons, and $M_{Ti,tot}=(k_B T_{i,down} - k_B T_{i,up})/(\sigma_i m_i c^2)$ for protons, where the subscripts 'up' (for upstream) and 'down' (for downstream) refer to the region in which the temperature is computed. Analogous ratio $M_{Te,irr}$, $M_{Ti,irr}$, $M_{Te,ad}$, and $M_{Ti,ad}$ characterize the irreversible (i.e., associated with genuine increase and entropy) and adiabatic (i.e., resulting from adiabatic compression) contributions to the total heating.

We identify downstream cells by using a particle mixing criterion between the two sides of the current sheet. Particles that originate above y=0 (top of the domain) are tagged, to distinguish them from particles originating below y=0 (bottom of the domain). The figure below shows the ratio of top to total number density. Away from the current sheet, i.e., in the blue and red regions, there is no mixing between the two populations. Particles from the two sides of the current sheet get mixed as they enter the reconnection layer; the region with the greatest amount of mixing is shown in white/light yellow. We compute the ratio of top particle density to total particle density in each cell. If this ratio in a given cell exceeds a chosen threshold, and is below the complementary threshold, then the cell is counted as one where plasma has reconnected (i.e., the cell belongs to the reconnection downstream). Cells belonging to the upstream are identified by a similar criterion; if mixing between the two populations is low, (or high) enough, the cells is counted as belonging to the upstream. This technique is similar to that used in Daughton et al (2014).

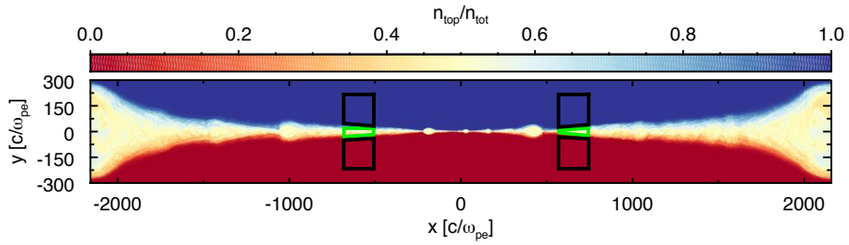

4 Results: Reconnection at Low and High β_i

The physics of reconnection shows a marked difference between low- and high-β_i regimes. In the figure below, we show a direct comparison between one low-β_i and one high-β_i simulation. The left column refers to β_i=0.0078, whereas β_i=0.5 for the right column. In both cases, σ_w=0.1. In the top row, we show the profiled along x of the outflow velocity for protons (red) and electrons (blue). The horizontal dashed lines show the Alfvén limit, $|v_{out}/v_A|$=1. We show in the middle row of panels the x-profile of the dimensionless electron temperature in the upstream (magenta) and downstream (green). Here, vertical dotted lines indicate the regions in the downstream used to calculate heating efficiencies. In the bottom row, we show 2D plots of the logarithm of electron dimensionless temperature.

We find that electrons move slightly faster than protons in the vicinity of the central X-point, but at larger distances the speeds of the two species are the same, and they saturate at a fixed fraction of the Alfvén limit.

The secondary magnetic islands present in the low-β_i simulation (panel (c)) are correlated with spikes in the downstream electron temperature (see the peak near x=-500 c/ω_{pe} in panel (b); ω_{pe} here is the electron plasma frequency, so that c/ω_{pe} is the electron skin depth). Aside from the temperature spikes at low β_i, the temperature profiles demonstrate that, far enough from the central X-point, the electron temperature is nearly uniform.

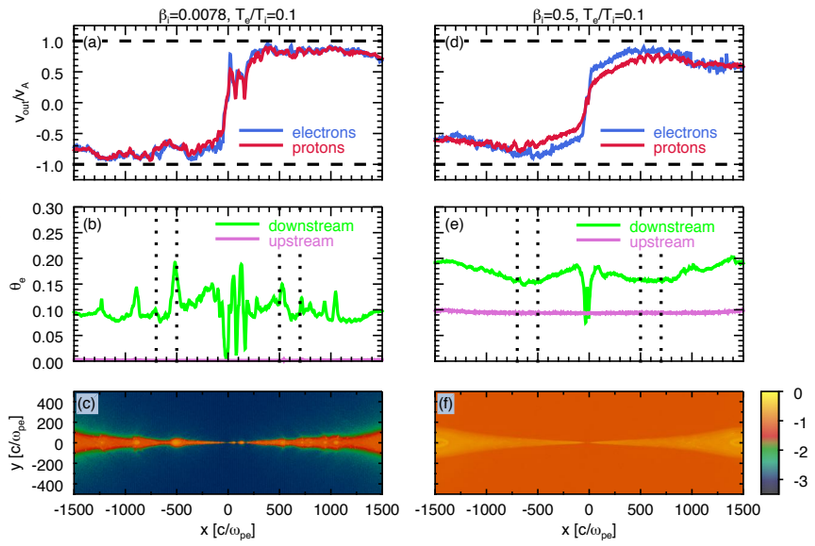

5 Results: Dependence of Heating on β_i, σ_w, and m_i/m_e

In the figure below, we show the mass ratio dependence of heating efficiencies: (a) electron total, (b) electron adiabatic, (c) electron irreversible, (d) proton total, (e) proton adiabatic, and (f) proton irreversible, for T_e/T_i=1 simulations with mass ratios m_i/m_e=10 (dotted), 25 (dashed), and 1836 (solid). Points in panels (a)-(c) are colored according to electron dimensionless temperature in the upstream (see color bar to the right of panel (c)), and points in panels (d)-(f) are colored according to proton dimensionless temperature in the upstream (color bar is to the right of panel (f)). The irreversible heating is remarkably independent of mass ratio at high β_i(=2), while at low β_i, the irreversible electron heating efficiency decreases with increasing mass ratio.

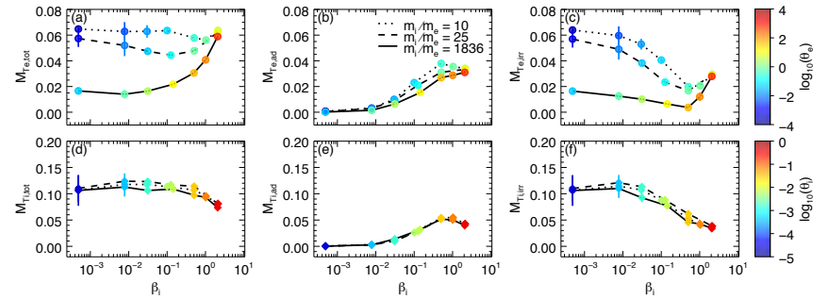

We show, in the figure below, the dependence of the heating efficiencies on magnetization σ_w (normalized to the enthalpy density), with a layout similar to the above figure: (a) electron total, (b) electron adiabatic, (c) electron irreversible, (d) proton total, (e) proton adiabatic, and (f) proton irreversible. We fix T_e/T_i=1 and m_i/m_e=1836 and vary the magnetization σ_w=0.1 (green), 0.3 (purple), 1 (brown), 3 (magenta), 10 (black). Points in panels (a)-(c) are colored according to the upstream electron dimensionless temperature (color bar is to the right of panel (c)), and points in panels (d)-(f) are colored according to the upstream proton dimensionless temperature (color bar is to the right of panel (f)).

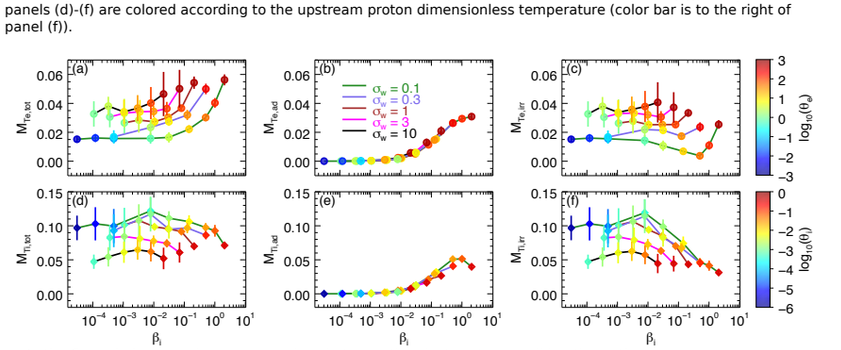

In the figure below, we show a comparison between the electron-to-overall heating ratio $q_{ue,tot}=M_{ue,tot}/(M_{ue,tot}+M_{ui,tot})$ between our simulations with m_i/m_e=1836 and T_e/T_i=1 (filled circles with error bars) and the best-fitting formula $q_{ue,fit}=(1/2)\exp[-(1-\beta_i/\beta_{i,max})^{3.3}/(1+1.2\,\sigma_w^{0.7})]$, where $\beta_i\le\beta_{i,max}=1/4\sigma_w$; the fitting formula is shown by solid curves. We show the dependence on (a) plasma-β_i and (b) magnetiation σ_w. In panel (a), the different colors represent magnetizations σ_w=0.1 (green), 0.3 (purple), 1 (brown), 3 (magenta), and 10 (black). In panel (b), the color coding of the curves is indicated in the legend (from cyan to red for increasing β_i), while the color of the filled points refers to the color bar to the right of panel (b). In both panels (a) and (b), the black dotted line at $q_{ue,tot}$=0.5 shows the limit of comparable heating efficiencies between electrons and protons, as expected when $\beta_i\to\beta_{i,max}$ (regardless of σ_w) or $\sigma_w\gg 1$ (independently of β_i). In panel (c), we show the betai dependence of downstream proton-to-electron skin depth ratio $(c/\omega_{pi})/(c/\omega_{pe})$, for magnetizations σ_w=0.1 (green), 0.3 (purple), 1 (brown), 3 (magenta), and 10 (black). For these simulations, the upstream electron-to-proton temperature is T_e/T_i=1, and m_i/m_e=1836.

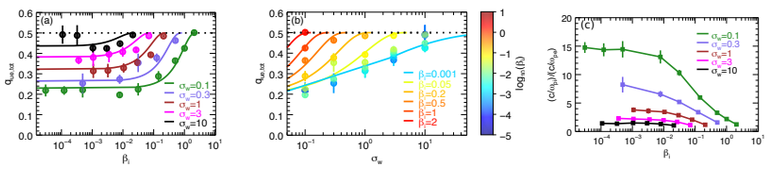

6 Conclusions

We show that heating in the high-β_i regime is primarily dominated by adiabatic compression, while for low β_i the heating is genuine, in the sense that it is associated with an increase in entropy. Protons are heated much more efficiently than electrons at low and moderate β_i (by a factor of ~7), whereas the electron and proton heating efficiencies become comparable at β_i~2 (if T_e/T_i=1). We find that comparable heating efficiencies between electrons and protons are achieved when the scale separation between the two species in the reconnection exhaust approaches unity, so that the electron-proton plasma effectively resembles an electron-positron fluid. This occurs at high β_i for low magnetizations, or regardless of β_i at high magnetizations.

This investigation provides important insights into the physics of low-luminosity accretion flows, such as the accretion disk of Sgr A*. Our results can be used to provide general relativistic MHD simulations of accretion flows with the subgrid physics of energy partition between electrons and protons.

7 References

Abramowicz, M. A. M. A., Chen, X., Kato, S., Lasota, J.-P. J.-P., & Regev, O. 1995, ApJL, 438, 8
Ball, D., Özel, F., Psaltis, D., Chan, C.-k., & Sironi, L. 2017, arXiv:1705.06293v1
Ball, D., Özel, F., Psaltis, D., & Kwan Chan, C. 2016, ApJ, 826, 77
Buneman, O. 1993, Computer Space Plasma Physics (Tokyo: Terra Scientific), 67
Chael, A. A., Narayan, R., & Sądowski, A. 2017, MNRAS, 470, 2367
Dahlin, J. T., Drake, J. F., & Swisdak, M. 2014, PhPl, 21, 092304Daughton, W., Nakamura, T. K. M.,
Karimabadi, H., Roytershteyn, V., & Loring, B. 2014, PhPl, 21
Guo, F., Li, X., Li, H., et al. 2016, ApJ, 818, L9
Hoshino, M., Hiraide, K., & Mukai, T. 2001, EP&S, 53, 627
Haggerty, C. C., Shay, M. A., Drake, J. F., Phan, T. D., & McHugh, C. T. 2015, GeoRL, 42, 9657
Jaroschek, C. H., Treumann, R. A., Lesch, H., & Scholer, M. 2004, PhPl, 11, 1151
Le, A., Egedal, J., & Daughton, W. 2016, PhPl, 23, 1
Li, X., Guo, F., Li, H., & Li, G. 2015, ApJ, 811, L24a
Li, X., Guo, F., Li, H., & Li, G. 2017, ApJ, 843, 21
Loureiro, N. F., Schekochihin, A. A., & Zocco, A. 2013, PhRvL, 111, 025002
Narayan, R., & Yi, I. 1994, ApJ, 428, 1316
Narayan, R., & Yi, I. 1995a, ApJ, 444, 231
Narayan, R., & Yi, I. 1995b, ApJ, 452, 710
Numata, R., & Loureiro, N. F. 2015, JPlPh, 81, 305810201
Yuan, F., & Narayan, R. 2014, ARA&A, 52, 529
Yuan, F., Quataert, E., & Narayan, R. 2003, ApJ, 598, 301
Quataert, E., Dorland, W., & Hammett, G. W. 2002, ApJ, 577, 524
Ressler, S. M., Tchekhovskoy, A., Quataert, E., Chandra, M., & Gammie, C. F. 2015, MNRAS, 454, 1848
Ressler, S. M., Tchekhovskoy, A., Quataert, E., & Gammie, C. F. 2017, MNRAS, 467, 3604
Riquelme, M. A., Quataert, E., Sharma, P., & Spitkovsky, A. 2012, 50
Riquelme, M. A., Quataert, E., & Verscharen, D. 2015, ApJ, 800, 27
Sądowski, A., Wielgus, M., Narayan, R., et al. 2017, MNRAS, 466, 705
Schoeffler, K. M., Drake, J. F., & Swisdak, M. 2011, ApJ, 743, 70
Schoeffler, K. M., Drake, J. F., Swisdak, M., & Knizhnik, K. 2013, ApJ, 764, 126
Shay, M. A., Haggerty, C. C., Phan, T. D., et al. 2014, PhPl, 21
Sironi, L. 2015, ApJ, 800, 89
Sironi, L., & Narayan, R. 2015, ApJ, 800, 88
Spitkovsky, A. 2005, in AIP Conf. Proc. 801 (Melville, NY: AIP), 345
Werner, G. R., Uzdensky, D. A., Begelman, M. C., Cerutti, B., & Nalewajko, K. 2016, arXiv:1612.04493